Active tectonics of the South Chilean marine fore arc (35°S–40°S)

Jacob Geersen,[1] Jan H. Behrmann,[1,2] David Völker,[1] Sebastian Krastel,[2] César R. Ranero,[3] Juan Diaz-Naveas,[4] and Wilhelm Weinrebe[1,2]

Received 11 August 2010; revised 3 March 2011; accepted 11 March 2011; published 8 June 2011.

[1] The South Chilean marine fore arc (35°S–40°S) is separated into four tectonic segments, Concepción North, Concepción South, Nahuelbuta, and Tolten (from north to south). These are each characterized by their individual tectonic geomorphology and reflect different ways of mechanical and kinematic interaction of the convergent Nazca and South American plates. Splay faults that cut through continental framework rock are seismically imaged in both Concepción segments and the Tolten Segment. Additionally, the Concepción South Segment exhibits prominent upper plate normal faults. Normal faults apparently relate to uplift caused by sediment underthrusting at depth. This has led to oversteepening and gravitational collapse of the marine fore arc. There is also evidence for sediment underthrusting and basal accretion to the overriding plate in the Tolten Segment. There, uplift of the continental slope has created a landward inclined seafloor over a latitudinal distance of 50 km. In the Nahuelbuta Segment transpressive upper plate faults, aligned oblique to the direction of plate motion, control the seafloor morphology. Based on a unique acoustic data set including >90% of bathymetric coverage of the continental slope we are able to reveal an along-strike heterogeneity of a complexly deformed marine fore arc which had escaped attention in previous studies that only considered the structure along transects normal to the plate margin.

Citation: Geersen, J., J. H. Behrmann, D. Völker, S. Krastel, C. R. Ranero, J. Diaz-Naveas, and W. Weinrebe (2011), Active tectonics of the South Chilean marine fore arc (35°S–40°S), *Tectonics*, *30*, TC3006, doi:10.1029/2010TC002777.

1. Introduction

[2] Marine fore-arc regions along convergent margins exhibit a variety in morphotectonic styles, as they are located within the tectonically most active plate-boundary environments. Active fault systems in the subsurface produce different morphologic features at the seafloor that can be visualized by acoustic imaging. This includes thrust ridges, fault escarpments, sedimentary basins, mass wasting structures and submarine canyons. As fore arcs in convergent plate boundary settings can be treated as critical Coulomb wedges [e.g., *Davis et al.*, 1983], any deformation will reflect changes in space and time of mechanical properties (e.g., friction along the plate boundary, internal strength, pore fluid pressure). To elucidate this the South Chilean fore arc is an interesting study area as it shows a pronounced along-strike segmentation in terms of earthquake rupture [*Lomnitz*, 1970; *Kelleher*, 1972; *Comte et al.*, 1986; *Campos et al.*, 2002; *Ruegg et al.*, 2009], seismicity [*Bohm et al.*, 2002; *Haberland et al.*, 2006], gravity anomalies [*Hackney et al.*, 2006; *Tašárová*, 2007], and topography [*Rehak et al.*, 2008]. Here we report the results of recent high-resolution multibeam bathymetric mapping of the continental slope in combination with reflection seismic data, reflecting a complex pattern of deformation in time and space.

[3] On land, an along-strike segmentation has been described in the rear part of the South Chilean fore arc between 36°S and 41°S; segmentation is reflected by changes in topography, distribution of young sedimentary basins, gravity anomalies and uplift rates [*Hackney et al.*, 2006; *Rehak et al.*, 2008; *Melnick et al.*, 2009; *Heberer et al.*, 2010]. Some of the segment boundaries coincide with boundaries of earthquake rupture zones [*Melnick et al.*, 2009]. This study shows and analyses high-resolution multibeam bathymetric data (predominantly collected during the last decade [e.g., *Flueh and Grevemeyer*, 2005; *Weinrebe and Schenk*, 2006; *Flueh and Bialas*, 2008]) in conjunction with reflection seismic data (part of them previously discussed by *Bangs and Cande* [1997]) that have been reprocessed [*Diaz-Naveas*, 1999]. We use this data set for a joint interpretation of subsurface structures and their corresponding seafloor expressions. We focus on the morphotectonic along-strike segmentation of the marine fore arc and how it is controlled by splay and normal faulting, basal and frontal sediment accretion, and upper plate structures. We further discuss possible controls for the generation of large upper plate normal faults.

[1] Collaborative Research Center (SFB) 574, Leibniz Institute of Marine Sciences at University of Kiel (IFM-GEOMAR), Kiel, Germany.
[2] Leibniz Institute of Marine Sciences at University of Kiel (IFM-GEOMAR), Kiel, Germany.
[3] ICREA, Barcelona Center for Subsurface Imaging, Instituto de Ciencias del Mar, CSIC, Barcelona, Spain.
[4] Escuela de Ciencias del Mar, Pontificia Universidad Catolica de Valparaiso, Valparaíso, Chile.

0278-7407/11/2010TC002777

1.1. Geologic and Tectonic Setting

[4] The tectonic framework of the South Chilean fore arc is controlled by the subduction of the Nazca Plate under the South American Plate at a present rate of 6.6 cm/yr and a convergence azimuth of about 80° (Figure 1) [*Angermann et al.*, 1999]. Oblique orientation of ocean plate isochrones results in a northward increase in plate age at the trench of about 1 Ma/100km [*Tebbens and Cande*, 1997]. The most prominent morphologic feature on the Nazca Plate in the region 35°S–40°S is the Mocha Fracture Zone (Figure 1) that intersects the trench slightly south of 38°S. Together with the Valdivia Fracture Zone (south of 40°S) the Mocha Fracture Zone separates young (0–25 Ma) oceanic lithosphere to the south from old (30–35 Ma) oceanic lithosphere to the north. In the marine fore arc no morphologic expression is visible that correlates with the projection of the Mocha Fracture Zone. There are speculations that the high relief of the Mocha Fracture Zone acts as barrier for the rupture of the 2010 Mw 8.8 Maule earthquake [*Contreras-Reyes et al.*, 2010]. Apart from the Mocha Fracture Zone no major topographic features are found on the oceanic plate in the region of this study.

[5] Until at least the middle Miocene [*Kukowski and Oncken*, 2006], or even until the Pliocene [*Melnick and Echtler*, 2006a] the marine fore arc of the study area has experienced subduction erosion. Since then, at least partial sediment accretion resulted in the buildup of an accretionary prism in the region between 33°S, where the Juan-Fernandez Ridge collides with the lower fore arc, and the Chile Triple Junction at 46.5°S [e.g., *Behrmann et al.*, 1994; *Bangs and Cande*, 1997; *Ranero et al.*, 2006]. However, the area in the close vicinity of the triple junction is currently not accreting [*Behrmann and Kopf*, 2001]. Nevertheless, accretion continues active south of the Chile Triple Junction [*Ranero et al.*, 2006]. At the latitudes of our study the change from subduction erosion to sediment accretion may have occurred during the onset of glaciation in the Patagonian Andes about 6 Ma ago, resulting in increased sediment flux to the trench [e.g., *Bangs and Cande*, 1997; *Melnick and Echtler*, 2006a]. Today, the trench fill thickness in the study area varies between 1500 m in the south and 2000 m in the north [*Diaz-Naveas*, 1999; *Ranero et al.*, 2006; *Völker et al.*, 2006]. Within the trench, a northward transport of sediment is described between 33°S and 42°S along a northward dipping trench-parallel axial channel that cuts down up to about 200 m into the trench fill [*Thornburg and Kulm*, 1987; *von Huene et al.*, 1997; *Völker et al.*, 2006].

[6] Five major submarine canyons incise the continental margin in the working area. From north to south these are the Itata, BioBio, Paleo-Pellahuen, Tolten/Imperial and CalleCalle Canyons (Figure 2). While the Paleo-Pellahuen Canyon seems to be a relict feature, and Itata Canyon is not present on the lower continental slope, the BioBio, Tolten/

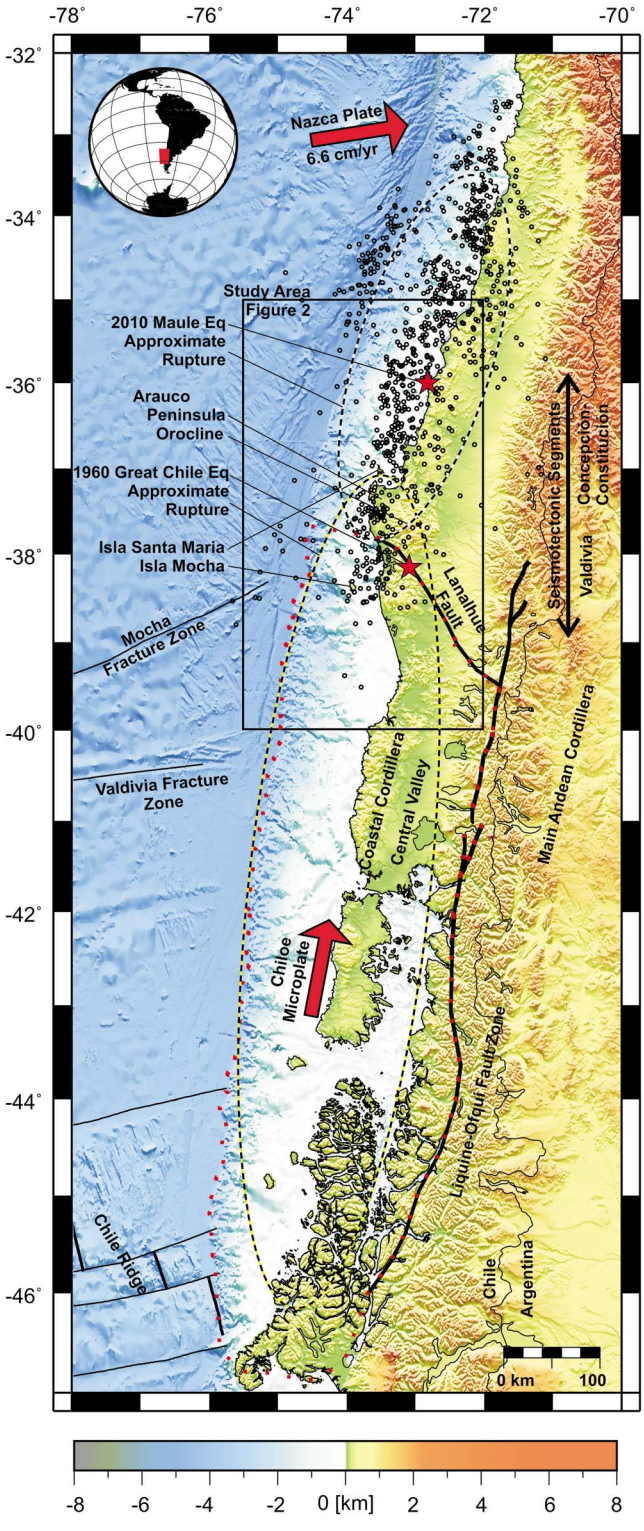

Figure 1. Overview map of south central Chile and western Argentina (data from GEBCO_08 Grid; version 20091120, http://www.gebco.net). Positions of the Liquine-Ofqui Fault Zone and the Lanalhue Fault are redrawn from *Melnick and Echtler* [2006b] and *Melnick et al.* [2009]. Boundaries of the Chiloe Microplate are indicated by red dotted line. Approximate convergence directions of the Nazca Plate and the Chiloe Microplate are displayed by red arrows. The epicenter locations of the 1960 Mw 9.5 Great Chile and the recent (27 February 2010) Mw 8.8 Maule earthquake are indicated by red stars. Approximate rupture areas of the two earthquakes are encircled by black and yellow and black and white lines. Open black circles are aftershocks of the Maule earthquake recorded in the period 27 February to 8 March 2010 (U.S. Geological Survey; http://www.usgs.gov).

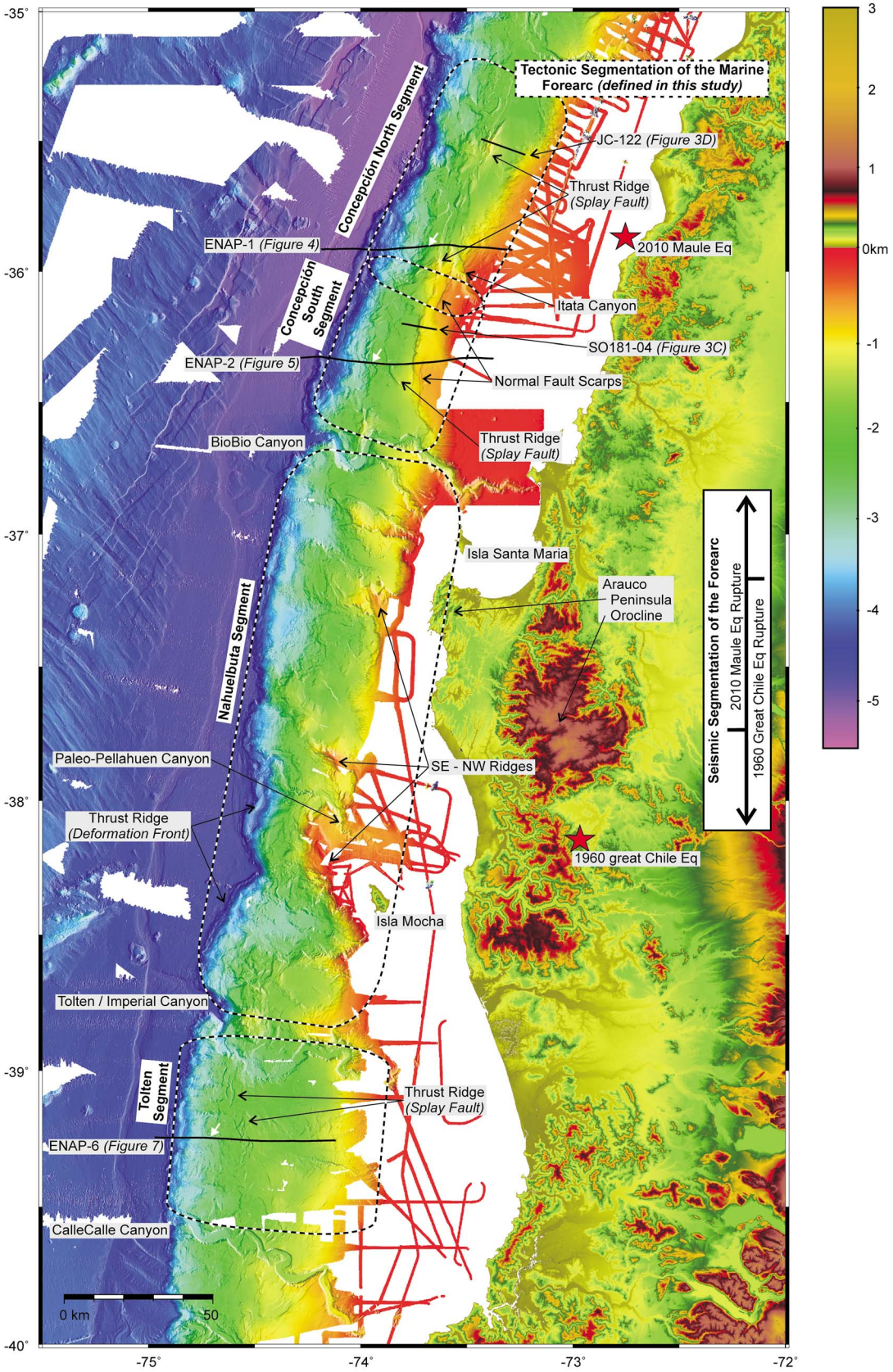
Tectonic Segmentation of the Marine Forearc (defined in this study)
Concepción North Segment
Concepción South Segment
Nahuelbuta Segment
Tolten Segment
JC-122 (Figure 3D)
Thrust Ridge (Splay Fault)
2010 Maule Eq
ENAP-1 (Figure 4)
Itata Canyon
SO181-04 (Figure 3C)
ENAP-2 (Figure 5)
Normal Fault Scarps
BioBio Canyon
Thrust Ridge (Splay Fault)
Isla Santa Maria
Arauco Peninsula Orocline
Seismic Segmentation of the Forearc
2010 Maule Eq Rupture
1960 Great Chile Eq Rupture
Paleo-Pellahuen Canyon
SE - NW Ridges
Thrust Ridge (Deformation Front)
1960 great Chile Eq
Isla Mocha
Tolten / Imperial Canyon
Thrust Ridge (Splay Fault)
ENAP-6 (Figure 7)
CalleCalle Canyon
0 km
50
-35°
-36°
-37°
-38°
-39°
-40°
-75°
-74°
-73°
-72°
3
2
1
0km
-1
-2
-3
-4
-5

Figure 2

Imperial and CalleCalle Canyons are considered to be currently active. These three canyons represent major and long-living sediment feeders to the trench [*Rehak et al.*, 2008]. Their activity is evident from their sheer sizes as they cut up to 1000 m deep into the continental slope. All three canyons are directly connected to major river systems draining parts of the Main Andean Cordillera and the Coastal Cordillera. At the canyon mouths there are prominent submarine fans [*Thornburg and Kulm*, 1987; *Völker et al.*, 2006; *Heberer et al.*, 2010].

[7] The continental fore arc and the magmatic arc are divided into three geomorphologic and tectonic provinces, the Coastal Cordillera, the Central Valley, and the Main Cordillera of the Andes (Figure 1). The most prominent structural feature in the Main Cordillera is the Liquine-Ofqui Fault Zone (LOFZ). The LOFZ is a longitudinal deep rooted fault system, which has been active in transpressional dextral mode since the Pliocene [*Hervé*, 1994; *Cembrano et al.*, 2000; *Thomson*, 2002; *Rosenau et al.*, 2006]. It decouples the Chiloe Microplate from the rest of the South American Plate (Figure 1). The Chiloe Microplate is a northward translating crustal sliver. Its northern edge is the Lanalhue Fault near 38°S [*Lavenu and Cembrano*, 1999; *Rosenau et al.*, 2006]. Kinematic modeling of the LOFZ predicts a long-term (6 Ma) shear rate of 32 ± 6 mm/yr in the southern domain (42°S–46°S) and 13 ± 3 mm/yr in the northern domain (38°S–42°S) [*Rosenau et al.*, 2006]. However, the recent strike-slip rate of the LOFZ is as low as 6.5 mm/yr according to GPS data [*Wang et al.*, 2007], which might be either caused by a slowdown of strike slip or by partial locking of the fault.

[8] Collision of the Chiloe Microplate with the South American Plate in the region of the Arauco Peninsula is a likely cause for transpressional faults (e.g., Lanalhue Fault) that dissect the fore arc in southeast-northwest direction (Figure 1) [*Melnick and Echtler*, 2006b; *Melnick et al.*, 2009]. Uplift of the continental fore arc and the islands of Santa Maria and Mocha (Figure 1) is interpreted as a result of active shortening across these faults [*Melnick et al.*, 2009], which has been inferred from inversion of fore-arc basins [*Melnick and Echtler*, 2006a], reorganization of river networks [*Rehak et al.*, 2008], and uplifted and tilted marine terraces [*Kaizuka et al.*, 1973; *Melnick et al.*, 2006]. Uplift rates are 0.8–5.5 mm/yr since the late Pleistocene [*Kaizuka et al.*, 1973; *Melnick et al.*, 2009] at Arauco Peninsula.

1.2. The Significance of Marine Fore Arcs for the Tectonic Evolution of Active Continental Margins

[9] In the marine fore arc, material is transferred from the oceanic to the continental plate by frontal or basal accretion. However, material can also be offscraped from the continental plate by subduction of slope sediment and tectonic erosion [*von Huene and Scholl*, 1991; *Clift and Vannucchi*, 2004]. Sediment piles transported into the subduction zone constrain strength and frictional behavior of the plate interface, thus influencing the rupture of great subduction zone earthquakes [e.g., *Ruff*, 1989; *Tichelaar and Ruff*, 1991]. Basal accretion induces local uplift of the fore arc [*Kopp et al.*, 2000; *Kukowski et al.*, 2001]. Furthermore, compression and shortening of the fore arc can cause the generation of splay faults, very long thrust faults that rise from the subduction plate boundary megathrust and intersect the seafloor [*Moore et al.*, 2007]. Splay faults are commonly located near the updip limit of the seismogenic zone [e.g., *Kimura et al.*, 2007; *Moore et al.*, 2007; *Collot et al.*, 2008] and may contribute to the generation of destructive tsunamis [e.g., *Moore et al.*, 2007].

1.3. Seismotectonic Segmentation of the South Chilean Margin

[10] Along the Chilean margin repeated great subduction earthquakes (Mw > 8.5) have defined distinct seismotectonic segments [*Lomnitz*, 1970, 2004; *Kelleher*, 1972; *Comte et al.*, 1986; *Campos et al.*, 2002; *Ruegg et al.*, 2009]. Two of these segments are located in the study area (Figures 1 and 2). The Valdivia Segment in the south was last affected by the Mw 9.5 Great Chile earthquake on 22 May 1960. This event ruptured about 1000 km of the Nazca–South America plate boundary thrust, and resulted in up to 5.7 m vertical coastal uplift. The last event that ruptured the Concepción-Constitución Segment in the north occurred on the 27 February 2010 with Mw 8.8. This earthquake is the second largest in the 21st century so far, and the fifth largest ever instrumentally recorded (U.S. Geological Survey; http://www.usgs.gov). The hypocenter of the main shock is at 35.9°S, 72.7°W at about 35 km depth, and rupture propagated northward and southward, defining a rupture area that extends along the marine fore arc between 33°S and 38.5°S (Figure 1) [e.g., *Moreno et al.*, 2010]. At least for these two earthquakes the rupture areas overlap in the region of the Arauco Peninsula (Figures 1 and 2) [*Barrientos and Ward*, 1990; *Lomnitz*, 2004; *Moreno et al.*, 2010].

[11] In this study we identify and discuss the role of splay faults in the marine fore arc of the areas that were ruptured during the 1960 Great Chile and 2010 Maule earthquakes. At least, part of the plate boundary coseismic movement may have been transferred into these fault systems. Fore-arc compression and uplift across the splay faults may have been responsible for the Pacific-wide tsunamis following the events.

2. Data Acquisition and Processing

2.1. Bathymetric Data

[12] In the region 35°S–40°S, high-resolution multibeam bathymetric data covers most of the South Chilean marine fore arc (Figure 2). Data has been collected in recent years by German, Chilean, French, and English research vessels

Figure 2. Combined bathymetric and topographic map (topographic data from the Shuttle Radar Topography Mission [*Farr et al.*, 2007]) of the study area. The four defined tectonic segments that are discussed in this study are encircled by black and white lines. Seismic lines are indicated by black lines. White arrows pointing on the seismic lines indicate the transition from rough to smooth seafloor that is interpreted as accretionary prism–continental framework rock boundary. The epicenter locations of the 1960 Mw 9.5 Great Chile and the recent (27 February 2010) Mw 8.8 Maule earthquake are indicated by red stars.

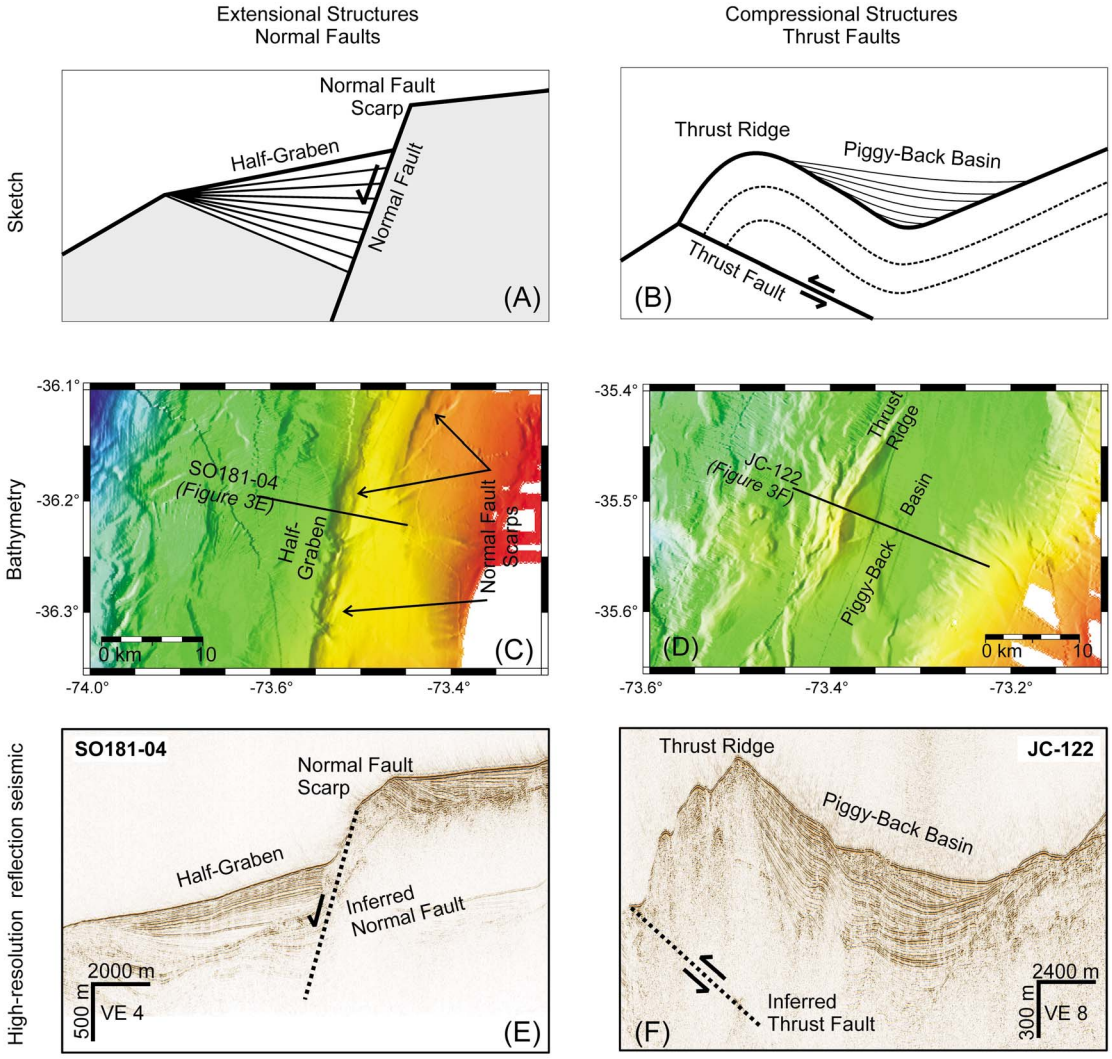

Figure 3. (a and b) Geometry of thrust and normal faults and (c and d) their bathymetric expressions. (e and f) Different basin structures created by thrust and normal faulting imaged by high-resolution reflection seismic data (compare Figure 2 for location of high-resolution reflection seismic lines).

[e.g., *Flueh and Grevemeyer*, 2005; *Weinrebe and Schenk*, 2006; *Flueh and Bialas*, 2008]. Different multibeam systems were used including the old Seabeam "classic" with 16 beams, Atlas Hydrosweep DS with 59 beams, Seabeam 1050 with 108 beams, as well as modern Kongsberg EM120 systems with 191 beams. Bathymetric data is presented here in synoptic and interpreted form for the first time.

2.2. Reflection Seismic Data

[13] Six multichannel reflection seismic lines with penetration of up to 12 s two-way traveltime (TWT), were acquired in 1988 onboard R/V Conrad for Empresa Nacional del Petroleo (ENAP) [*Bangs and Cande*, 1997; *Diaz-Naveas*, 1999]. In this study we show and reinterpret parts of three of these lines (ENAP-1, ENAP-2 and ENAP-6) following the naming scheme of *Diaz-Naveas* [1999]. Seismic line ENAP-1 is line 728 shown by *Bangs and Cande* [1997] and line ENAP-6 is line 732. Seismic line ENAP-2 was not presented by *Bangs and Cande* [1997]. Lines are oriented approximately east to west, perpendicular to the direction of maximum slope angle. An array of 10 air guns with an overall volume of 80 l was used as seismic source. Signals were recorded with a 3000 m long streamer consisting of 240 channels with a group spacing of 12.5 m that nominally yields a 6.25 m common midpoint spacing, but for processing the data were rebinned to 25 m spacing. Reprocessing included velocity analysis, normal moveout corrections, f-k filtering multiple attenuation, deconvolution, stacking, and finite differences poststack time migration. For a more detailed description of the individual processing steps the reader is referred to *Diaz-Naveas* [1999].

[14] In addition to the ENAP seismic data two extracts from high-resolution seismic lines (SO181-04 and JC-122) are shown in Figures 3e and 3f, in order to elucidate the effect of thrust and normal faulting on the uppermost sedimentary layers. Seismic line SO181-04 was collected during R/V *Sonne* cruise 181-1b using a 16 channel, 100 m long hydrophone array and an SSI GI seismic source (2 * 1.72 l)

[*Flueh and Grevemeyer*, 2005]. Line JC-122 was recorded during RRS James Cook cruise 23b with a 65 m four channel streamer and a 4.1 l GI gun [*Flueh and Bialas*, 2008]. Peak frequencies of both lines are centered at around 70 Hz.

3. Data Description and Interpretation

3.1. Compressional and Extensional Structures as Visualized by Bathymetric and Reflection Seismic Data

[15] Deep penetrating reflection seismic lines have been used successfully in the interpretation of marine fore-arc structures. However, the increasing amount of high-resolution reflection seismic and bathymetric data becoming available during the last years has created the chance for evaluation techniques of activity, style and geometry based on the surface expressions of individual fault systems. Figure 3 highlights how different tectonic deformation structures, i.e., thrust systems indicating a compressional regime and normal faults indicating extension, can be identified in both types of acoustic data sets.

[16] If sub seafloor data are absent, bathymetric data can be used for a first-order discrimination between thrust and normal faulting, although there may be uncertainties. However, there are characteristic geomorphic seafloor expressions created by individual fault types. While a thrust ridge and its subjacent strata are inclined in two opposite directions (Figures 3b and 3d), the seabed on both sides of a normal fault scarp usually dips trenchward (Figures 3a and 3c). With high-resolution reflection seismic data available it is clear that both types of faults create distinctive associated basin structures that allow discrimination. In case of a thrust fault, the basin is generated in the hanging wall above and behind the thrust ridge and is termed piggyback basin. Strata are often inclined landward and upslope and the depocenter moves away from the thrust ridge with time, as the overthrust unit is moved up the thrust ramp (Figure 3f). In contrast, normal faulting creates a basin that overlies the fault plane in the footwall, and the pattern of strata is such as to show greatest thickness next to the fault scarp, akin to a fill of a half-graben (Figure 3e). Interpretation of the bathymetric data in terms of active faulting style in this paper was made with reference to these geomorphic features.

3.2. Segmentation of the Marine Fore Arc

[17] The analysis of high-resolution multibeam bathymetric and reflection seismic data reveals some fundamental along-strike variations concerning the morphotectonics of the marine fore arc in the region 35°S–40°S. To account for these variations, the study area is divided into four major tectonic segments (Figure 2): Concepción North, Concepción South, Nahuelbuta, and Tolten (from north to south). Tectonic segments in the marine fore arc are defined according to similarities in their seafloor geomorphology (e.g., ridges, escarpments, slope gradients, and slope aspect) and subsurface structures (e.g., splay faults and normal faults). Boundaries between the tectonic segments are drawn where morphologic parameters change. In any case, the defined tectonic segments and above all segment boundaries are not adopted from the terrestrial fore arc, but do coincide partially with proposed segmentation on land. Furthermore, tectonic segment boundaries do not reflect the seismotectonic segmentation as the boundary between the Concepción-Constitución and the Valdivia seismotectonic segment is located within one of the defined tectonic segments (Nahuelbuta Segment). The geomorphology and subsurface structures of the individual segments are described in the following to provide the base for a discussion of the tectonic development of the study area.

3.2.1. Concepción North Segment

[18] The area east of the deformation front is characterized by margin-parallel thrust ridges that rise up to 600 m above the flat trench floor (Figure 2). In seismic line ENAP-1 (Figure 4) the frontal thrust, which geometrically forms the Nazca–South America plate boundary, dips landward and is traced to the top of the subducting oceanic basement (TOB). The TOB is present at 6.5–8.0 s TWT depth, indicated by a strong, subhorizontal reflection. A series of minor thrust ridges underlain by thrust faults that separate individual thrust sheets (Figure 4) can be traced within the accretionary prism upslope from the deformation front to a water depth of around 2500 m. Similar to *Bangs and Cande* [1997], we interpret the part of the seismic line between the deformation front and CMP 3325 as the active accretionary prism. Toward the continent, thrust ridges in the accretionary prism become less obvious in the bathymetric data (Figure 2), and the reflection seismic data do not reveal details of the internal fore arc structure (Figure 4), as bedding parallel reflectors are no longer imaged due to progressive folding and imbrication.

[19] The transition from the accretionary prism to the continental framework rock is located around CMP 3325 (Figure 4). It is described by two main characteristics. First, landward of the transition a high-amplitude reflection is observed about 0.5–1.7 s TWT below the seafloor (Figure 4) and interpreted as the top of the framework rock (TFR). The TFR can be traced toward the eastern end of the seismic line. The transition is further characterized by a significant change in the nature of the seafloor (indicated by white arrow; Figure 2). A smooth and undisturbed seafloor is visible in the bathymetric and seismic data on the upper continental slope, where continental framework rock is present. Contrary, the seafloor in the accretionary prism appears quite rough and disturbed (Figures 2 and 4).

[20] At the upper continental slope two 0.5 s TWT high thrust ridges are identified in the seismic line (Figure 4). In the bathymetric data they coincide with a north-south trending thrust ridge up to 500 m in height which splits into two branches at its southern end (where seismic line ENAP-1 is situated; Figures 2, 3d and 4b). This thrust ridge extends for about 80 km along the continental slope and is visible all along the Concepción North Segment. Around 35.75°S it is breached by a channel structure associated with the Itata Canyon (Figure 2). At the position of seismic line ENAP-1 (Figure 4), this ridge is underlain by two landward dipping reflections which we interpret as splay faults. Splay faults seem to continue toward greater depth. However, as the exact location of the plate boundary is not resolved in this part of the seismic line, it is unclear where they splay away from the plate boundary thrust. Thrust faulting in this case does not only lead to the build up of the thrust ridge at the seafloor but also seems to displace the TFR along the fault planes.

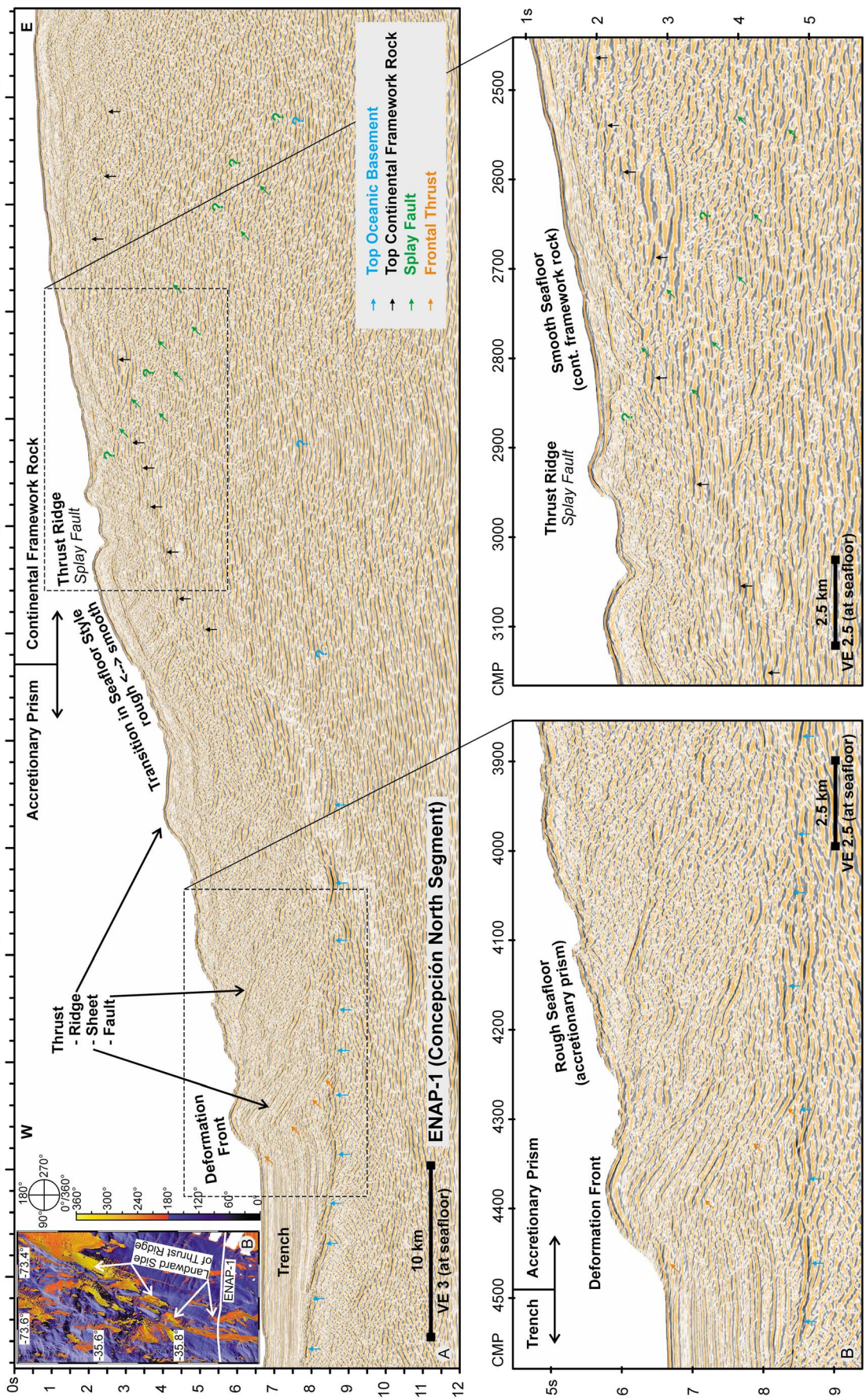

Figure 4. (a) Seismic line ENAP-1 crossing the Concepción North Segment (corresponds to line 728 of *Bangs and Cande* [1997]); see Figure 2 for location. (b) Slope aspect map for the area of the outstanding thrust ridge imaged at the upper continental slope of the Concepción North Segment. The thrust ridge can be identified due to its landward inclined side.

3.2.2. Concepción South Segment

[21] The lower continental slope resembles that of the Concepción North Segment with thrust sheets above landward dipping thrust faults resulting in trench-parallel thrust ridges (Figures 2 and 5). The individual thrust sheets build the accretionary prism, which extends from the deformation front about 20 km landward, up to a water depth around 3000 m. The frontal thrust is traced from the deformation front toward a depth of 7.5 s TWT, about 0.4 s TWT above the TOB. The TOB is imaged as an undulating, high-amplitude reflection between 7.0 and 8.0 s TWT. Landward from the deformation front to CMP 3400, high-amplitude reflections, imaged around a depth of 7.0–7.5 s TWT, delineate the décollement. These reflections occur in continuation of the lower trench sediment fill and parallel the TOB reflection. This indicates that in the Concepción South Segment a section of about 0.4 s TWT of trench sediment is being underthrust beneath the overriding plate.

[22] Along seismic line ENAP-2 (Figure 5) the transition from the accretionary prism to the continental framework rock is situated at the TFR reflection at around CMP 2750 (Figure 5). The TFR is identified as a high-amplitude reflection about 1.0–2.2 s TWT below the seafloor reflection, and traced toward the eastern end of the seismic line. Again, the transition is described by a change in seafloor style visible in the bathymetric data (indicated by white arrow; Figure 2). A smooth seafloor is present in the framework rock part of the margin and a rough and disturbed seafloor in the area of the accretionary prism.

[23] While the upper continental slope of the Concepción North Segment is dominated by the occurrence of a prominent thrust ridge, the Concepción South Segment is characterized by escarpments, up to 500 m high, that dip seaward (Figures 2 and 3c) with slope angles of up to 30°. The most prominent escarpment is intersected by seismic lines ENAP-2 (Figure 5) and SO181-04 (Figure 3e). The escarpment coincides with a small slope basin on its seaward side containing a fill of well-stratified sediments up to 0.4 s TWT thick. Basin geometry suggests that this is a half-graben structure overlying a seaward dipping normal fault. The slope basin shows thicker sediments on the hanging wall side of the fault than on the footwall side indicating that this normal fault is a growth fault. It is difficult to trace the exact location of the fault plane in the seismic data. However, there is no displacement found in the TFR that occurs in line with the scarp of the normal fault. Thus, normal faulting seems to occur only above the framework rock.

[24] At the escarpment of the above described normal fault a landward dipping high-amplitude reflection is observed in seismic line ENAP-2 (Figure 5) that crops out at the seafloor around CMP 3450. We interpret this reflection as splay fault, as it is inferred to a depth of about 7.2 s TWT where the main plate boundary is expected. There is another landward dipping high-amplitude reflection observed in seismic line ENAP-2 which crops out at the seafloor around CMP 3050 (Figure 5). We also interpret it as splay fault as it is traced to the plate interface at around CMP 3800. The surface expression of this fault is a 350 m high north-south trending thrust ridge which is observed over a distance of about 20 km (Figures 2 and 5b). Along both splay faults the TFR is displaced up to 0.6 s TWT.

3.2.3. Nahuelbuta Segment

[25] In the Nahuelbuta Segment, seafloor morphology is more complex in comparison to the Concepción North and Concepción South Segments (Figures 2 and 6). As there is no seismic line available for this segment, we concentrate on the analysis of high-resolution multibeam bathymetry. Frontal accretion of sediments is indicated by margin-parallel thrust ridges in the lower fore arc (Figures 2 and 6a).

[26] Different from the northern two segments which host north-south striking thrust ridges and normal faults, the morphologic features in the Nahuelbuta Segment are preferentially aligned oblique to the direction of the Nazca Plate motion. Three southeast-northwest trending ridges (marked by black arrows; Figure 6a) are visible in the bathymetry. The enormous extend of the surface area that is affected by the three ridges becomes obvious in the slope aspect map (Figure 6b) that highlights regions with a northeast (landward) inclined seafloor (yellow to red). In this view, three southeast-northwest elongated areas with a northeast inclined seafloor are evident (marked by black arrows; Figure 6b). They extend throughout the whole Nahuelbuta Segment, reaching from the shelf to the lower continental slope. However, these areas of northeast inclined seafloor do not occur in the area occupied by trench-parallel thrust ridges at the lowermost continental slope.

[27] Figure 6 further shows the positions of deeply rooted continental upper plate faults on land (e.g., Morguilla Fault, Mocha-Villarica Fault Zone, Lanalhue Fault) drawn after *Melnick and Echtler* [2006b] and *Melnick et al.* [2009]. Seaward extrapolations of these faults coincide with the southeast-northwest trending ridges described above. If we follow the line of reasoning taken so far, southeast-northwest aligned ridges in the marine fore arc are related to compressive, or dextrally transpressive faulting. This is a scenario that would be in line with the inferences made about the deformation in front of the northward moving Chiloe Microplate [*Melnick and Echtler*, 2006b; *Melnick et al.*, 2009].

[28] In addition to the above described southeast-northwest trending morphologic features the Nahuelbuta Segment hosts two prominent slope embayments (Figure 6a). Slope embayments are found south of the BioBio Canyon and north of the Tolten/Imperial Canyon and are possibly the result of slope failure. Due to the alignment of their sidewalls (east-west, roughly in the direction of maximum slope angle) these slope embayments can be distinguished from the southeast-northwest trending ridge structures.

3.2.4. Tolten Segment

[29] Bathymetric data exhibits rather smooth seafloor morphology in the Tolten Segment compared to the three segments described above (Figure 2). Along seismic line ENAP-6 (Figure 7), the region between CMP 4150 and 4900 is interpreted as accretionary prism (about 15 km in width). Individual thrust ridges cannot be clearly identified in bathymetric (Figure 2) and seismic (Figure 7) data. A frontal thrust is visible but does only extend to a subbottom depth of about 0.6 s TWT (Figure 7). The lack of distinct thrust sheets indicates that sediments which are incorporated into the frontal accretionary prism probably deform by folding, obliterating the layer signature seen in the seismic section seaward of the frontal thrust.

[30] On seismic line ENAP-6 (Figure 7), a band of strong reflections between CMP 3800 and 4800 describes

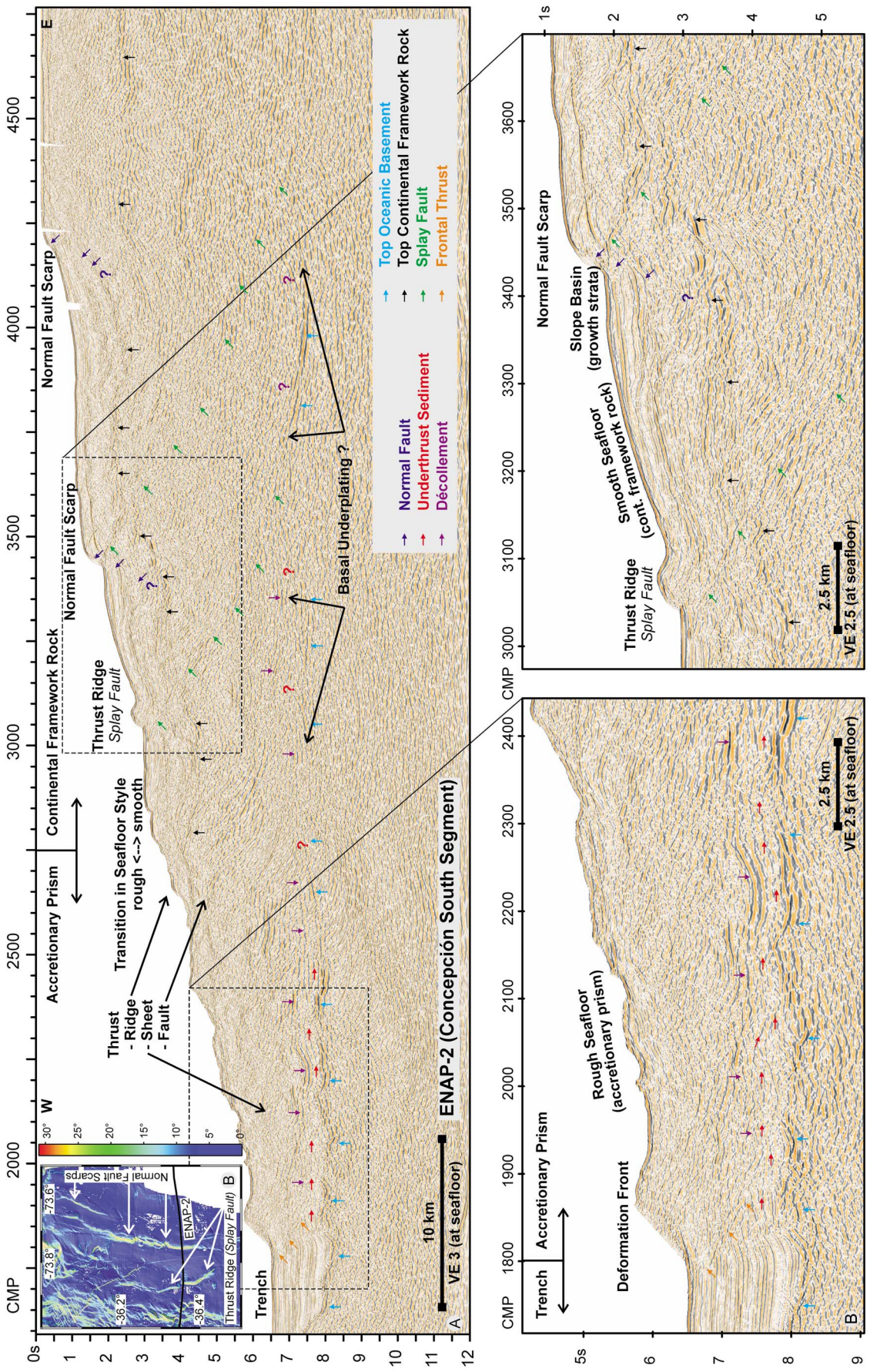

Figure 5. (a) Seismic line ENAP-2 crossing the Concepción South Segment; see Figure 2 for location. (b) Slope angle map for the area of the outstanding normal faults imaged at the upper continental slope of the Concepción South Segment.

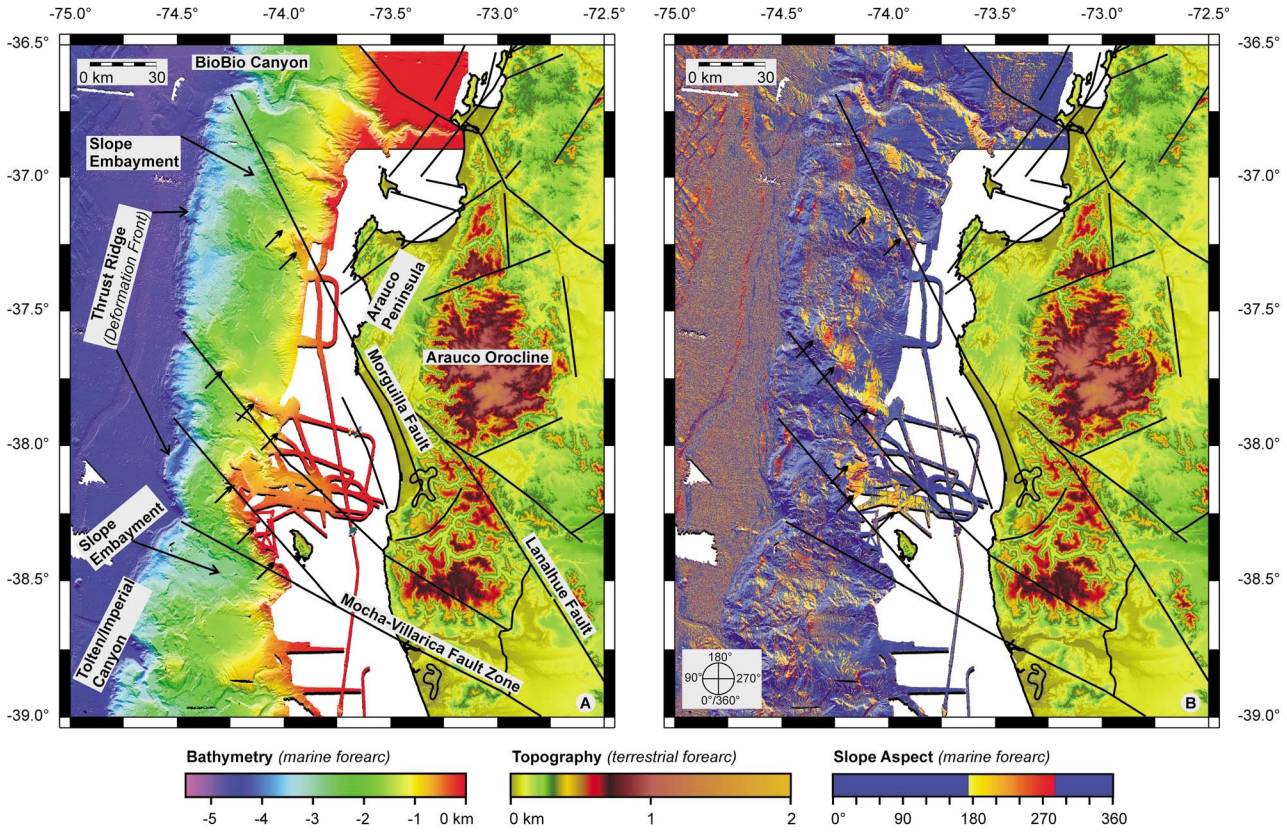

Figure 6. (a) Combined topographic (topographic data from the Shuttle Radar Topography Mission [*Farr et al.*, 2007]) and bathymetric map of the Nahuelbuta Segment. Continental, upper plate faults (solid black lines) are redrawn from *Melnick and Echtler* [2006b] and *Melnick et al.* [2009]. Black arrows indicate southeast-northwest trending ridges found in the marine fore arc. (b) Combined topographic and slope aspect map of the same area. Southeast-northwest elongated areas in the marine fore arc that host a northeast inclined seafloor are marked by black arrows. These features are interpreted to represent the surface expressions of the marine continuation of continental, upper plate faults.

the décollement. The décollement is found about 0.5–1.0 s TWT above the undulating high-amplitude reflector, which we interpret as TOB. Similar to *Bangs and Cande* [1997] we attribute this reflection pattern to the presence of a thick section of sediment that is being underthrust beneath the marine fore arc. Around CMP 3800, the coherent parallel reflection pattern of the underthrust sediments disappears. However, in this part of the seismic line the depth of the underthrust sediments coincides with the area where the first seafloor multiple is located (partly removed during seismic processing). Thus, we are not able to conclude if this is a tectonic feature or an imaging problem. Nevertheless, from the updomed morphology of the slope we infer that some of the underthrust sediment has been basally accreted to the overriding plate here.

[31] The transition from the accretionary prism to the continental framework rock is more difficult to identify than in the above described segments. The TFR can be traced as a high-amplitude band of reflections from the eastern end of the seismic line to CMP 3700. Westward of CMP 3700 high-amplitude reflections are observed to CMP 4150, which could represent faulted framework rock, however this is not clear from the seismic data. To locate the boundary between accretionary prism and framework rock we consider the bathymetric data (Figure 2) which shows a transition from a smooth and undisturbed seafloor to a more rough seafloor around 3000 m water depth (indicated by white arrow). As for the northern two seismic lines (ENAP-1, Figure 4 and ENAP-2, Figure 5) the change in seafloor roughness observed in the bathymetric data correlates well with the extend of the framework rock observed in the seismic data we place the accretionary prism–framework rock boundary in the Tolten Segment to this position. This implies that along seismic line ENAP-6 (Figure 7) framework rock may extend to CMP 4150 and, thus, about 20 km further seaward than proposed by *Bangs and Cande* [1997]. In the region around CMP 3200 the TFR forms a 1.5 s TWT deep morphological depression, which probably is the remnant of an abandoned canyon system now filled by sediments covering the whole of the upper marine fore arc.

[32] Around CMP 3600 a ridge about 0.4 s TWT in height is identified in the seismic data (Figure 7). In the bathymetric data this feature coincides with a laterally continuous band of small ridges around 2200 m water depth (Figure 2). In seismic line ENAP-6 (Figure 7) the ridge is underlain by

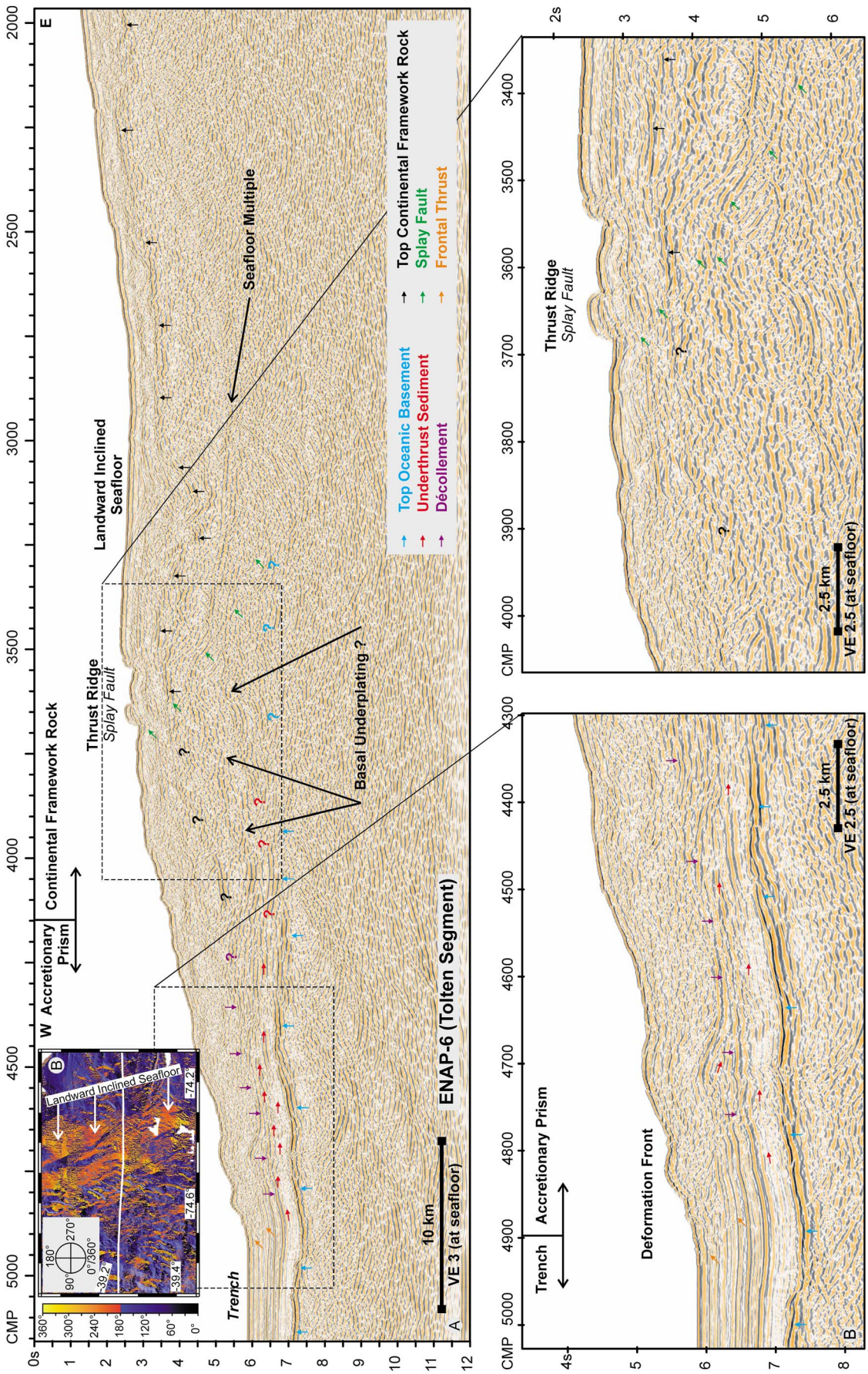

Figure 7. (a) Seismic line ENAP-6 crossing the Tolten Segment (corresponds to line 732 of *Bangs and Cande* [1997]); see Figure 2 for location. (b) Slope aspect map for the Tolten Segment highlighting the landward inclined seafloor at the upper continental slope.

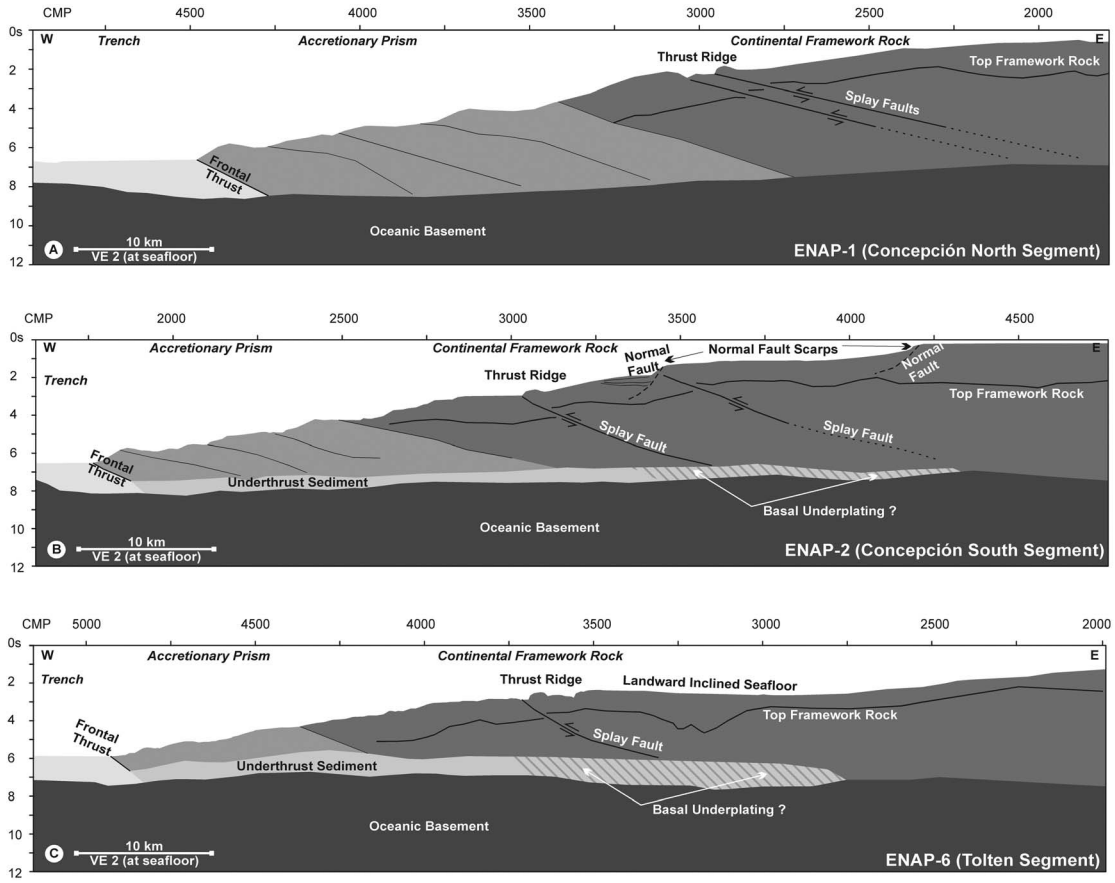

Figure 8. Line drawings of seismic lines (a) ENAP-1, (b) ENAP-2, and (c) ENAP-6. See Figure 2 for locations of seismic lines.

a landward dipping high-amplitude reflection which we interpret as splay fault.

[33] Landward from the splay fault outcrop, the transition to an almost undeformed upper fore-arc slope, without major tectonic features at the seafloor, occurs (Figures 2 and 7). Furthermore, the upper slope is characterized by very low slope gradients and as described by *Bangs and Cande* [1997], is inclined at small angles (<4°) toward the continent over a latitudinal distance of about 50 km (Figure 7b). This is a feature unique to the Tolten Segment, and we will discuss the significance below.

4. Discussion

[34] Based on the analysis of high-resolution multibeam bathymetric and reflection seismic data we demonstrate distinct segmentation of the South Chilean marine fore arc, which relates to active tectonics. We now discuss a number of controlling factors for the observed variations in the tectonic geomorphology of the four identified segments of the plate margin (Figure 2). The single segments are not treated individually. Instead, the discussion is structured according to the different modes of deformation active in several segments. We consider how splay and normal faulting affects the morphology of the continental slope and address the question why the prominent faults are formed. Furthermore, we discuss the impact of basal and frontal sediment accretion and the role of upper plate structures on the morphology of the continental slope. Figure 8 presents cartoon interpretations of the three ENAP seismic lines that we integrate with the observed geomorphologic variations in the study area.

4.1. Splay and Normal Faults in the Study Area and Their Relation to Seafloor Expression

[35] Splay faults are imaged in the Concepción North, Concepción South and Tolten Segments (Figures 4, 5, 7 and 8). Although no direct control on the activity of these faults is possible with our data, their surface expressions (thrust ridges) found in the three tectonic segments indicate recent activity. The transfer of coseismic fault movement into the overriding plate across the splay faults leads to long-term shortening and steepening of the whole fore-arc wedge and results in the development of prominent thrust ridges at the upper continental slope (Figures 2 and 8), forming bathymetric features rising up to 500 m above the surrounding seafloor.

[36] Whereas the Concepción North and the Tolten Segments exhibit one prominent splay fault system, the tectonic setting of the Concepción South Segment appears more complex. Here, two splay faults as well as prominent normal faults are imaged at the upper continental slope (Figures 2, 5 and 8b), with at least one normal fault interpreted as a

growth fault. Both splay faults are imaged as fairly continuous seismic reflections, which can be traced from the seafloor to greater depth. The prominent thrust ridge at the seafloor above the western splay fault indicates that they are active faults. However, the growth strata, on the hanging wall of the lowermost normal fault also indicates some amount of young if not recent activity of this structure. An overprinting relationship which would help to evaluate the activity of the different faults over time cannot be established because fault planes of thrust and normal faults do not intersect at depth (Figure 5).

[37] Contrasting to the splay faults, normal faults are only traced within the upper about 1.5 s TWT of the subsurface above the continental framework rock. Similar extensional structures are found on the shelf and upper continental slope off Oregon [*McNeill et al.*, 1997], where they developed due to unstable underlying sediment packages. Although there is no geologic unit known so far from the South Chilean fore arc that would be especially prone to unstable gravitational sliding, it is interesting to note that the positions of normal faults within the South Chilean marine fore arc are similar to those found off Oregon.

[38] Similar to the splay faults, normal faulting strongly modifies continental slope morphology by producing up to 500 m high escarpments and local slope angles exceeding 30° (Figures 2, 5 and 8b). Splay faults in the study area are exclusively located within continental framework rock. This is interesting, as in other convergent margins such structures have been identified either within accretionary complexes, or at the boundary between accretionary prism and continentally derived framework rock [e.g., *Collot et al.*, 2008]. The South Chilean case is different, as the position of splay faults seems to be independent of changes in fore-arc material.

4.2. Causes for Large-Scale Normal Faulting in the Concepción South Segment

[39] We now discuss possible controls on the generation of observed normal faults in the Concepción South Segment. Uplift of the marine fore arc, resulting in oversteepening and gravitational collapse, can be caused by a number of underlying tectonic processes. These are (1) shortening and uplift across upper plate compressional faults, (2) subduction of major topographic features such as seamounts or basement ridges [*Lallemand et al.*, 1994; *Hampel et al.*, 2004], (3) steepening of the margin due to progressive subduction erosion [*von Huene and Ranero*, 2003; *Sallarès and Ranero*, 2005; *Ranero et al.*, 2006] and (4) basal underplating of trench sediments [*Kopp et al.*, 2000; *Kukowski et al.*, 2001].

[40] Splay faults imaged in the Concepción North, Concepción South and Tolten Segments account for significant shortening and uplift of the marine fore arc. However, normal faults are restricted to the Concepción South Segment and do not occur in the other two segments. Thus, we consider thrust faulting and induced shortening not to be the direct cause for the generation of these normal faults. The subduction of major topographic features such as seamounts or basement ridges does not seem to play a role for normal faulting as the Nazca Plate at these coordinates is devoid of any major topographic features. Steepening of the margin related to progressive subduction erosion as proposed for Northern Chile [*von Huene and Ranero*, 2003; *Sallarès and Ranero*, 2005; *Ranero et al.*, 2006] cannot explain observed normal faults as the southern Chilean margin is currently in an accretionary mode.

[41] Excluding the above discussed processes, basal underplating of trench sediment might be the only mechanism responsible for the generation of observed normal faults. Indeed, seismic line ENAP-2 (Figure 5, Concepción South Segment) shows a thick section of trench sediment (35 km length; about 0.8 s TWT thick) which is imaged above the subducting oceanic basement. Underthrust sediments can be traced to around CMP 3400 (Figure 5) but are not well resolved in the seismic data further landward. Thus, it is possible that they are underplated below the overriding plate eastward from CMP 3400. This process could lead to an uplift of the upper slope and shelf area with observed normal faults resulting from gravitational collapse of the flanks of the uplifted region.

[42] *Wang and Hu* [2006] expanded the theory of critical tapered Coulomb wedges [*Davis et al.*, 1983] by considering stress changes during earthquake cycles. In their work they showed that normal faulting in the region landward of the accretionary prism is possible during the coseismic period. As normal faulting in our study area is restricted to the Concepción South Segment we suggest that coseismic relaxation is not its ultimate cause, but might contribute to the growth of normal faults over time.

4.3. Sediment Accretion in the Tolten Segment and the Implications for Seafloor Geomorphology

[43] In the Tolten Segment a rather small accretionary prism and a thick (about 1 s TWT) section of underthrust sediment are observed (Figures 7 and 8c). The upper slope in the Tolten Segment forms an anomaly compared to the rest of the study area as it is inclined toward the continent over a latitudinal distance of about 50 km (Figures 2, 7 and 8c). This anomaly in slope direction was already observed by *Bangs and Cande* [1997] who speculated that it is caused by a change in upper plate rheology from soft accretionary prism material to a material that is able to transfer stress without deformation and act as rigid backstop. An additional explanation that may act simultaneously is provided by the thick sequence of underthrust sediment seen in Figure 7 between the frontal thrust and CMP 3800. Together with the operation of the splay fault, the underthrust sediment helps to jack up the fore arc around CMP 3800 to create the morphological high and the landward dipping slope. Movement along splay faults rooted in the plate boundary thrust alone is unlikely to create this type of seafloor morphology, as can be seen by comparing Figures 8a and 8c. Jacking up the fore arc above a thick underthrust sediment package also prevents oversteepened slopes on the upper continental slope and, thus, the operation of normal faults. As discussed above this process is important in keeping the fore arc critically tapered in the Concepción South Segment (Figure 8b), where only a thin package of sediments is being underthrust.

4.4. Controls on the Amount of Sediment Underthrusting

[44] Underthrusting of trench sediment in the study area is observed in the Concepción South and Tolten Segments,

and is absent in the Concepción North Segment. Interestingly, the segments where underthrusting takes place are those that are located close to or even host the deep sea fans of the BioBio, Tolten/Imperial and CalleCalle Canyons. The canyons are fed by onshore river systems with extensive sediment source areas in the Main Cordillera of the Andes and therefore provide an important source for sediments in the trench. Our first attempt to explain this by identifying a positive correlation between the volume of sediment that is underthrusted, and the volume of sediment in the trench failed. Against our expectations the correlation is negative: In segments where sediment is underthrusted, i.e., those segments that contain deep sea canyon fans, the sediment thickness in the trench is small. Sediment thickness is greatest in the Concepción North Segment (about 2.0 s TWT in ENAP-1; Figure 4) and smallest in the Tolten Segment (about 1.5 s TWT in ENAP-6; Figure 7). Thus, the thickness of the subduction channel seems to be independent of the thickness of the sedimentary trench fill. Trench fill thickness is not controlled by the position of submarine canyon fans.

[45] *Contreras-Reyes et al.* [2010] point to a general southward increase in the thickness of the subduction channel of southern Chile, taking into account the whole region from the Juan Fernandez Ridge to the Chile Triple Junction. They explain their observation by the reduced elasticity of the young (0–25 Ma) oceanic lithosphere in the south which favors a pronounced down-deflection at the trench due to sediment loading [*Contreras-Reyes and Osses*, 2010]. This might increase the initial angle of subduction compared to the old (30–35 Ma) oceanic lithosphere in the north and thus favors the formation of a thick subduction channel. However, this interpretation fails to explain observed variations in subduction channel thickness between the Concepción North (seismic line ENAP-1; Figure 4) and the Concepción South Segments (seismic line ENAP-2; Figure 5), where there are no large differences in age of the oceanic lithosphere. We thus suggest that along the southern Chile Trench there are important smaller (100 km) scale variations of surface processes that control the sediment delivery and deposition in the trench, and ultimately the amount of sediment to be subducted.

4.5. Active Tectonics of the Nahuelbuta Segment Controlled by Transpressive Upper Plate Structures and the Question of Seismotectonic Segmentation

[46] The tectonic geomorphology of the marine as well as the continental fore arc of the Nahuelbuta Segment differs fundamentally from the other segments discussed in this study. Continental geology was studied extensively in recent years [e.g., *Rehak et al.*, 2008; *Melnick et al.*, 2009] and based on the bathymetric data we now extend this work into the marine fore arc. Apart from the differences in the tectonic geomorphology it is interesting to note that the boundary between the Valdivia Seismotectonic Segment (1960 Great Chile earthquake) and the Concepción-Constitución Seismotectonic Segment (2010 Maule earthquake) is situated in the Nahuelbuta Segment (Figure 2), but does not coincide with either of its boundaries.

[47] Figure 6 gives an overview of major continental faults (solid black lines; redrawn from *Melnick and Echtler* [2006b] and *Melnick et al.* [2009]) which are caused by the northward movement of the Chiloe Microplate and its collision with the stable South American Plate. Based on seafloor morphology we infer that the observed southeast-northwest elongated areas in the marine fore arc that host a northeast inclined seafloor (Figures 2 and 6) are the surface expressions of the marine continuation of these important upper plate faults. This further explains why the northeast inclined seafloor disappears before reaching the interplate deformation front, as here the transition from the continental framework rock to the accretionary prism occurs, with the latter not affected by continental faults. Consequently, transpression across southeast-northwest trending crustal faults, as suggested for the Arauco Orocline [*Melnick et al.*, 2009], continues into the marine fore arc to the area where the transition from the upper slope to the accretionary prism occurs.

[48] Regarding the tectonic processes (i.e., transpression across upper plate faults), the tectonic geomorphology of the Nahuelbuta Segment is predominantly controlled by the overriding plate. This is in contrast to the other three tectonic segments defined in this study, where deformation processes in the plate boundary and its kinematics exert an overriding influence.

[49] For the Nahuelbuta Segment we show that continental upper plate faults are present as first-order tectonic features in the marine as well as the terrestrial fore arc in the area of the boundary between the Valdivia and the Concepción-Constitución Seismotectonic Segments. For the future it will be interesting to further investigate the potential influence of these faults in defining (limiting) earthquake rupture propagation.

5. Conclusions

[50] The South Chilean marine fore arc (35°S–40°S) comprises four segments of different geomorphology, structure and active tectonics: Concepción North, Concepción South, Nahuelbuta, and Tolten (from north to south). The northern study area (Concepción North and Concepción South Segments) shows prominent splay faults and outstanding thrust ridges on the upper continental slope. Splay faults are located within continental framework rock. In addition to splay faulting the Concepción South Segment exhibits major normal faults. Extension resulting in gravitational collapse of the marine fore arc is suggested as the result of sediment underthrusting, basal accretion and inferred uplift of the upper continental slope. Sediment underthrusting is also proposed for the Tolten Segment where inferred uplift of the marine fore arc generated a landward inclined seafloor over a latitudinal distance of about 50 km. Again, splay faulting indicates the transfer of coseismic fault movement into the overriding plate. Contrary to the other segments, the seafloor morphology in the Nahuelbuta Segment is controlled by transpressive structures in the overriding plate provoked by active northward movement of the Chiloe Microplate.

[51] **Acknowledgments.** We would like to thank the Editor Onno Oncken and reviewers Lisa McNeill and Nathan Bangs for their comments. We also thank Roland von Huene for fruitful discussions and suggestions on an earlier version of the manuscript. Some figures were drawn with the generic mapping tools. This publication is contribution 198 of the Sonderforschungsbereich 574 "Volatiles and Fluids in Subduction Zones" at Kiel University.

References

Angermann, D., J. Klotz, and C. Reigber (1999), Space-geodetic estimation of the Nazca–South America Euler vector, *Earth Planet. Sci. Lett.*, *171*(3), 329–334, doi:10.1016/S0012-821X(99)00173-9.

Bangs, N. L., and S. C. Cande (1997), Episodic development of a convergent margin inferred from structures and processes along the southern Chile margin, *Tectonics*, *16*, 489–503, doi:10.1029/97TC00494.

Barrientos, S. E., and S. N. Ward (1990), The 1960 Chile earthquake: Inversion for slip distribution from surface deformation, *Geophys. J. Int.*, *103*, 589–598, doi:10.1111/j.1365-246X.1990.tb05673.x.

Behrmann, J., and A. Kopf (2001), Balance of tectonically accreted and subducted sediment at the Chile Triple Junction, *Int. J. Earth Sci.*, *90*(4), 753–768, doi:10.1007/s005310000172.

Behrmann, J. H., S. D. Lewis, and S. C. Cande (1994), Tectonics and geology of spreading ridge subduction at the Chile Triple Junction: A synthesis of results from Leg 141 of the Ocean Drilling Program, *Geol. Rundsch.*, *83*(4), 832–852, doi:10.1007/BF00251080.

Bohm, M., S. Lüth, H. Echtler, G. Asch, K. Bataille, C. Bruhn, A. Rietbrock, and P. Wigger (2002), The Southern Andes between 36° and 40°S latitude: Seismicity and average seismic velocities, *Tectonophysics*, *356*(4), 275–289, doi:10.1016/S0040-1951(02)00399-2.

Campos, J., D. Hatzfeld, R. Madariaga, G. Lopez, E. Kausel, A. Zollo, G. Iannacone, R. Fromm, S. Barrientos, and H. Lyon-Caen (2002), A seismological study of the 1835 seismic gap in south-central Chile, *Phys. Earth Planet. Inter.*, *132*, 177–195, doi:10.1016/S0031-9201(02)00051-1.

Cembrano, J., E. Schermer, A. Lavenu, and A. Sanhueza (2000), Contrasting nature of deformation along an intra-arc shear zone, the Liquiñe-Ofqui fault zone, southern Chilean Andes, *Tectonophysics*, *319*(2), 129–149, doi:10.1016/S0040-1951(99)00321-2.

Clift, P., and P. Vannucchi (2004), Controls on tectonic accretion versus erosion in subduction zones: Implications for the origin and recycling of the continental crust, *Rev. Geophys.*, *42*, RG2001, doi:10.1029/2003RG000127.

Collot, J.-Y., W. Agudelo, A. Ribodetti, and B. Marcaillou (2008), Origin of a crustal splay fault and its relation to the seismogenic zone and underplating at the erosional north Ecuador–south Colombia oceanic margin, *J. Geophys. Res.*, *113*, B12102, doi:10.1029/2008JB005691.

Comte, D., A. Eisenberg, E. Lorca, M. Pardo, L. Ponce, R. Saragoni, S. K. Singh, and G. Suárez (1986), The 1985 central Chile earthquake: A repeat of previous great earthquakes in the region?, *Science*, *233*(4762), 449–453, doi:10.1126/science.233.4762.449.

Contreras-Reyes, E., and A. Osses (2010), Lithospheric flexure modelling seaward of the Chile trench: Implications for oceanic plate weakening in the Trench Outer Rise region, *Geophys. J. Int.*, *182*, 97–112.

Contreras-Reyes, E., E. R. Flueh, and I. Grevemeyer (2010), Tectonic control on sediment accretion and subduction off south central Chile: Implications for coseismic rupture processes of the 1960 and 2010 megathrust earthquakes, *Tectonics*, *29*, TC6018, doi:10.1029/2010TC002734.

Davis, D., J. Suppe, and F. A. Dahlen (1983), Mechanics of fold-and-thrust belts and accretionary wedges, *J. Geophys. Res.*, *88*(B2), 1153–1172, doi:10.1029/JB088iB02p01153.

Diaz-Naveas, J. L. (1999), Sediment subduction and accretion at the Chilean convergent margin between 35° and 40°S, Ph.D. thesis, Univ. of Kiel, Kiel, Germany.

Farr, T. G., et al. (2007), The Shuttle Radar Topography Mission, *Rev. Geophys.*, *45*, RG2004, doi:10.1029/2005RG000183.

Flueh, E. R., and J. Bialas (2008), Cruise report JC23: Chile-Margin-Survey 03.03.2008–18.04.2008, report, 242 pp., IFM-GEOMAR, Kiel, Germany.

Flueh, E. R., and I. Grevemeyer (2005), Cruise report SO 181 TIPTEQ (from the incoming plate to mega thrust earthquakes) 06.12.2004–26.02.2005, report, 533 pp., IFM-GEOMAR, Kiel, Germany.

Haberland, C., A. Rietbrock, D. Lange, K. Bataille, and S. Hofmann (2006), Interaction between forearc and oceanic plate at the south-central Chilean margin as seen in local seismic data, *Geophys. Res. Lett.*, *33*, L23302, doi:10.1029/2006GL028189.

Hackney, R. I., et al. (2006), The segmented overriding plate and coupling at the south-central Chilean Margin (36–42°S), in *The Andes: Active Subduction Orogeny*, edited by O. Oncken et al., pp. 355–374, Springer, Berlin.

Hampel, A., N. Kukowski, J. Bialas, C. Huebscher, and R. Heinbockel (2004), Ridge subduction at an erosive margin: The collision zone of the Nazca Ridge in southern Peru, *J. Geophys. Res.*, *109*, B02101, doi:10.1029/2003JB002593.

Heberer, B., G. Roser, J. H. Behrmann, M. Rahn, and A. Kopf (2010), Holocene sediments from the southern Chile Trench: A record of active margin magmatism, tectonics and palaeoseismicity, *J. Geol. Soc.*, *167*(3), 539–553, doi:10.1144/0016-76492009-015.

Hervé, F. (1994), The southern Andes between 39° and 44°S latitude: The geological signature of a transpressive tectonic regime related to a magmatic arc, in *Tectonics of the Southern Central Andes*, edited by K. J. Reuter, E. Scheuber, and P. J. Wigger, pp. 243–248, Springer, Berlin.

Kaizuka, S., T. Matsuda, M. Nogami, and N. Yonekura (1973), Quaternary tectonic and recent seismic crustal movements in the Arauco peninsula and its environs, central Chile, *Geogr. Rep. Tokyo Metrop. Univ.*, *8*, 1–49.

Kelleher, J. A. (1972), Rupture zones of large South American earthquakes and some predictions, *J. Geophys. Res.*, *77*(11), 2087–2103, doi:10.1029/JB077i011p02087.

Kimura, G., Y. Kitamura, Y. Hashimoto, A. Yamaguchi, T. Shibata, K. Ujiie, and S. Okamoto (2007), Transition of accretionary wedge structures around the up-dip limit of the seismogenic subduction zone, *Earth Planet. Sci. Lett.*, *255*(3–4), 471–484, doi:10.1016/j.epsl.2007.01.005.

Kopp, C., J. Fruehn, E. R. Flueh, C. Reichert, N. Kukowski, J. Bialas, and D. Klaeschen (2000), Structure of the Makran subduction zone from wide-angle and reflection seismic data, *Tectonophysics*, *329*(1–4), 171–191, doi:10.1016/S0040-1951(00)00195-5.

Kukowski, N., and O. Oncken (2006), Subduction erosion—The "normal" mode of fore-arc material transfer along the Chilean Margin?, in *The Andes: Active Subduction Orogeny*, edited by O. Oncken et al., pp. 217–236, Springer, Berlin.

Kukowski, N., T. Schillhorn, K. Huhn, U. von Rad, S. Husen, and E. R. Flueh (2001), Morphotectonics and mechanics of the central Makran accretionary wedge off Pakistan, *Mar. Geol.*, *173*(1–4), 1–19, doi:10.1016/S0025-3227(00)00167-5.

Lallemand, S. E., P. Schnürle, and J. Malavieille (1994), Coulomb theory applied to accretionary and nonaccretionary wedges: Possible causes for tectonic erosion and/or frontal accretion, *J. Geophys. Res.*, *99*(B6), 12,033–12,055, doi:10.1029/94JB00124.

Lavenu, A., and J. Cembrano (1999), Compressional- and transpressional-stress pattern for Pliocene and Quaternary brittle deformation in fore arc and intra-arc zones (Andes of central and southern Chile), *J. Struct. Geol.*, *21*(12), 1669–1691, doi:10.1016/S0191-8141(99)00111-X.

Lomnitz, C. (1970), Major earthquakes and tsunamis in Chile during the period 1535 to 1955, *Int. J. Earth Sci.*, *59*(3), 938–960, doi:10.1007/BF02042278.

Lomnitz, C. (2004), Major earthquakes of Chile: A historical survey, 1535–1960, *Seismol. Res. Lett.*, *75*(3), 368–378, doi:10.1785/gssrl.75.3.368.

McNeill, L. C., K. A. Piper, C. Goldfinger, L. D. Kulm, and R. S. Yeats (1997), Listric normal faulting on the Cascadia continental margin, *J. Geophys. Res.*, *102*(B6), 12,123–12,138, doi:10.1029/97JB00728.

Melnick, D., and H. P. Echtler (2006a), Inversion of forearc basins in south-central Chile caused by rapid glacial age trench fill, *Geology*, *34*(9), 709–712, doi:10.1130/G22440.1.

Melnick, D., and H. P. Echtler (2006b), Morphotectonic and geologic digital map compilations of the south-central Andes (36°–42°S), in *The Andes: Active Subduction Orogeny*, edited by O. Oncken et al., pp. 565–568, Springer, Berlin.

Melnick, D., B. Bookhagen, H. P. Echtler, and M. R. Strecker (2006), Coastal deformation and great subduction earthquakes, Isla Santa Maria, Chile (37°S), *Geol. Soc. Am. Bull.*, *118*(11–12), 1463–1480, doi:10.1130/B25865.1.

Melnick, D., B. Bookhagen, M. R. Strecker, and H. P. Echtler (2009), Segmentation of megathrust rupture zones from fore-arc deformation patterns over hundreds to millions of years, Arauco peninsula, Chile, *J. Geophys. Res.*, *114*, B01407, doi:10.1029/2008JB005788.

Moore, G. F., N. L. Bangs, A. Taira, S. Kuramoto, E. Pangborn, and H. J. Tobin (2007), Three-dimensional splay fault geometry and implications for tsunami generation, *Science*, *318*(5853), 1128–1131, doi:10.1126/science.1147195.

Moreno, M., M. Rosenau, and O. Oncken (2010), 2010 Maule earthquake slip correlates with pre-seismic locking of Andean subduction zone, *Nature*, *467*(7312), 198–202, doi:10.1038/nature09349.

Ranero, C. R., R. von Huene, W. Weinrebe, and C. Reichert (2006), Tectonic processes along the Chile convergent margin, in *The Andes: Active Subduction Orogeny*, edited by O. Oncken et al., pp. 91–121, Springer, Berlin.

Rehak, K., M. R. Strecker, and H. P. Echtler (2008), Morphotectonic segmentation of an active forearc, 37°–41°S, Chile, *Geomorphology*, *94*(1–2), 98–116, doi:10.1016/j.geomorph.2007.05.002.

Rosenau, M., D. Melnick, and H. Echtler (2006), Kinematic constraints on intra-arc shear and strain partitioning in the southern Andes between 38°S and 42°S latitude, *Tectonics*, *25*, TC4013, doi:10.1029/2005TC001943.

Ruegg, J. C., A. Rudloff, C. Vigny, R. Madariaga, J. B. de Chabalier, J. Campos, E. Kausel, S. Barrientos, and D. Dimitrov (2009), Interseismic strain accumulation measured by GPS in the seismic gap between Constitución and Concepción in Chile, *Phys. Earth Planet. Inter.*, *175*, 78–85, doi:10.1016/j.pepi.2008.02.015.

Ruff, L. J. (1989), Do trench sediments affect great earthquake occurrence in subduction zones?, *Pure Appl. Geophys.*, *129*(1–2), 263–282, doi:10.1007/BF00874629.

Sallarès, V., and C. R. Ranero (2005), Structure and tectonics of the erosional convergent margin off Antofagasta, north Chile (23°30′S), *J. Geophys. Res.*, *110*, B06101, doi:10.1029/2004JB003418.

Tašárová, Z. A. (2007), Towards understanding the lithospheric structure of the southern Chilean subduction zone (36°S–42°S) and its role in the gravity field, *Geophys. J. Int.*, *170*, 995–1014, doi:10.1111/j.1365-246X.2007.03466.x.

Tebbens, S. F., and S. C. Cande (1997), Southeast Pacific tectonic evolution from early Oligocene to present, *J. Geophys. Res.*, *102*(B6), 12,061–12,084, doi:10.1029/96JB02582.

Thomson, S. N. (2002), Late Cenozoic geomorphic and tectonic evolution of the Patagonian Andes between latitudes 42°S and 46°S: An appraisal based on fission-track results from the transpressional intra-arc Liquiñe-Ofqui fault zone, *Geol. Soc. Am. Bull.*, *114*(9), 1159–1173, doi:10.1130/0016-7606(2002)114<1159:LCGATE>2.0.CO;2.

Thornburg, T. M., and L. D. Kulm (1987), Sedimentation in the Chile Trench: Depositional morphologies, lithofacies, and stratigraphy, *Geol. Soc. Am. Bull.*, *98*(1), 33–52, doi:10.1130/0016-7606(1987)98<33:SITCTD>2.0.CO;2.

Tichelaar, B. W., and L. J. Ruff (1991), Seismic coupling along the Chilean subduction zone, *J. Geophys. Res.*, *96*(B7), 11,997–12,022, doi:10.1029/91JB00200.

Völker, D., M. Wiedicke, S. Ladage, C. Gaedicke, C. Reichert, K. Rauch, W. Kramer, and C. Heubeck (2006), Latitudinal variation in sedimentary processes in the Peru-Chile trench off central Chile, in *The Andes: Active Subduction Orogeny*, edited by O. Oncken et al., pp. 193–216, Springer, Berlin.

von Huene, R., and C. R. Ranero (2003), Subduction erosion and basal friction along the sediment-starved convergent margin off Antofagasta, Chile, *J. Geophys. Res.*, *108*(B2), 2079, doi:10.1029/2001JB001569.

von Huene, R., and D. W. Scholl (1991), Observations at convergent margins concerning sediment subduction, subduction erosion, and the growth of continental crust, *Rev. Geophys.*, *29*(3), 279–316, doi:10.1029/91RG00969.

von Huene, R., J. Corvalan, E. R. Flueh, K. Hinz, J. Korstgard, C. R. Ranero, W. Weinrebe, and CONDOR Scientists (1997), Tectonic control of the subducting Juan Fernández Ridge on the Andean margin near Valparaiso, Chile, *Tectonics*, *16*, 474–488, doi:10.1029/96TC03703.

Wang, K., and Y. Hu (2006), Accretionary prisms in subduction earthquake cycles: The theory of dynamic Coulomb wedge, *J. Geophys. Res.*, *111*, B06410, doi:10.1029/2005JB004094.

Wang, K., Y. Hu, M. Bevis, E. Kendrick, R. Smalley Jr., R. B. Vargas, and E. Lauría (2007), Crustal motion in the zone of the 1960 Chile earthquake: Detangling earthquake-cycle deformation and forearc-sliver translation, *Geochem. Geophys. Geosyst.*, *8*, Q10010, doi:10.1029/2007GC001721.

Weinrebe, W., and S. Schenk (2006), Cruise report M67/1 Chile-Margin-Survey 20.02–13.03.2006, report, 113 pp., IFM-GEOMAR, Kiel, Germany.

J. H. Behrmann, J. Geersen, D. Völker, and W. Weinrebe, Collaborative Research Center (SFB) 574, Leibniz Institute of Marine Sciences at University of Kiel (IFM-GEOMAR), Wischhofstr. 1-3, D-24148 Kiel, Germany. (jgeersen@ifm-geomar.de)

J. Diaz-Naveas, Escuela de Ciencias del Mar, Pontificia Universidad Catolica de Valparaiso, Av. Altamirano 1480, Casilla 1020, Valparaíso, Chile.

S. Krastel, Leibniz Institute of Marine Sciences at University of Kiel (IFM-GEOMAR), Wischhofstr. 1-3, D-24148 Kiel, Germany.

C. R. Ranero, ICREA, Barcelona Center for Subsurface Imaging, Instituto de Ciencias del Mar, CSIC, Pg. Maritim de la Barceloneta 37-49, E-08003, Barcelona, Spain.